ACS APPLIED MATERIALS & INTERFACES

Research Article

www.acsami.org

Small Molecules Based on Thieno[3,4-*c*]pyrrole-4,6-dione for High Open-Circuit Voltage (V_{OC}) Organic Photovoltaics: Effect of Different Positions of Alkyl Substitution on Molecular Packing and Photovoltaic Performance

Yoon Suk Choi,[†] Tae Joo Shin,[‡] and Won Ho Jo*[,†]

[†]Department of Materials and Engineering, Seoul National University, 1 Gwanak-ro, Gwanak-gu, Seoul 151-744, Korea

[‡]Pohang Accelerator Laboratory, Kyungbuk, Pohang 790-784, Republic of Korea

Supporting Information

ABSTRACT: Two different thienopyrroledione (TPD)-based small molecules (SMs) with different alkyl substitution positions were synthesized, and their photovoltaic properties are measured and compared to examine the effect of the alkyl substitution position on their optical, electrochemical, and photovoltaic properties. The use of TPD as an electron-accepting unit in conjugated SMs effectively lowers the highest occupied molecular orbital (HOMO) energy levels of the conjugated SMs and leads to high open-circuit voltage (V_{OC}). The two SMs with *n*-hexyl group substituted at different positions exhibit almost identical optical and electrochemical properties in the pristine state. However, the crystallographic and morphological characteristics of the two SMs are significantly different, because they are blended with $PC_{71}BM$. The SM in which *n*-alkyl groups are substituted at the central accepting unit exhibits a power conversion efficiency (PCE) of 6.0% with V_{OC} = 0.94 V, which is among the highest PCE values of TPD-based SM devices, whereas the SM with *n*-alkyl groups being substituted at the chain ends shows a moderate PCE value of 3.1%.

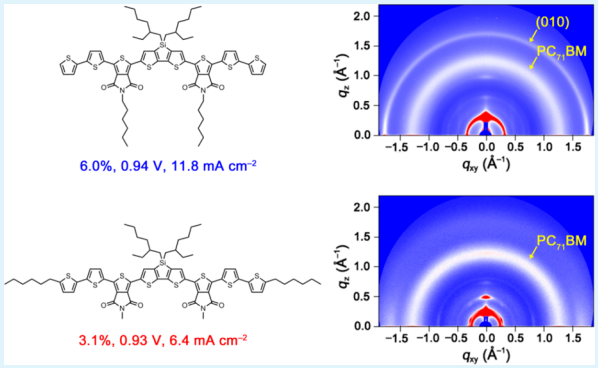

KEYWORDS: *thienopyrroledione, organic solar cells, small molecules, high V_{OC}, alkyl chain position*

1. INTRODUCTION

Recently, the power conversion efficiencies (PCEs) of solution-processed small molecule (SM)-based organic solar cells (OSCs) have steadily been increased, with efficicncies close to those of polymer solar cells (PSCs).[1−4] However, the overall performances of SM-based OSCs are still inferior to those of polymer counterparts. For high-performance SM-based OSCs, the strategies used for the design of high-performance conjugated polymers could also be applied to the molecular design of SMs. Therefore, the electron donor−acceptor (D−A)-type architecture that has been proven as the most effective method to achieve high-performance PSCs can also be utilized for the design of high-performance SMs.[5−12]

Thieno[3,4-*c*]pyrrole-4,6-dione (TPD) has been a promising moiety as an A unit[13−18] in D−A-type conjugated polymers, because its relatively strong electron accepting power leads to low frontier orbital energy levels of corresponding conjugated polymers, which is required for high open-circuit voltage (V_{OC}) in bulk heterojunction (BHJ) PSCs. Although it is generally accepted that the highest occupied molecular orbital (HOMO) energy level and the lowest unoccupied molecular orbital (LUMO) energy level of D−A-type conjugated molecules are governed mainly by the electronic properties of D and A units, respectively, exceptional but interesting results have been reported when a TPD unit is used as an A unit in D−A-type conjugated backbone: Both HOMO and LUMO levels are lowered when TPD is used as an A unit in D−A-type conjugated molecules. For instance, it has been reported that a low-bandgap polymer (PTB7), composed of benzoditihophene (BDT) and thieno[3,4-*b*]thiophene (TT) as the D and A units, respectively, exhibits HOMO and LUMO energy levels of −5.15 and −3.31 eV, respectively.[19] When the TT unit in PTB7 is replaced by a stronger electron accepting unit (TPD), the polymer (PBDTTPD) exhibits lower-lying HOMO and LUMO energy levels of −5.56 and −3.75 eV, respectively.[20] Another polymer (PDTSTPD) composed of dithieno[3,2-*b*:2′,3′-*d*]silole (DTS) as the D unit and TPD as the A unit also exhibits deep HOMO and LUMO energy levels of −5.57 and −3.88 eV, respectively.[21] It should be mentioned here that TPD-based molecules exhibit deeper HOMO energy levels,

Received: August 20, 2014
Accepted: October 21, 2014
Published: October 21, 2014

   dx.doi.org/10.1021/am505608s | *ACS Appl. Mater. Interfaces* 2014, 6, 20035−20042

Scheme 1. Synthetic Route of TPD-Based Small Molecules

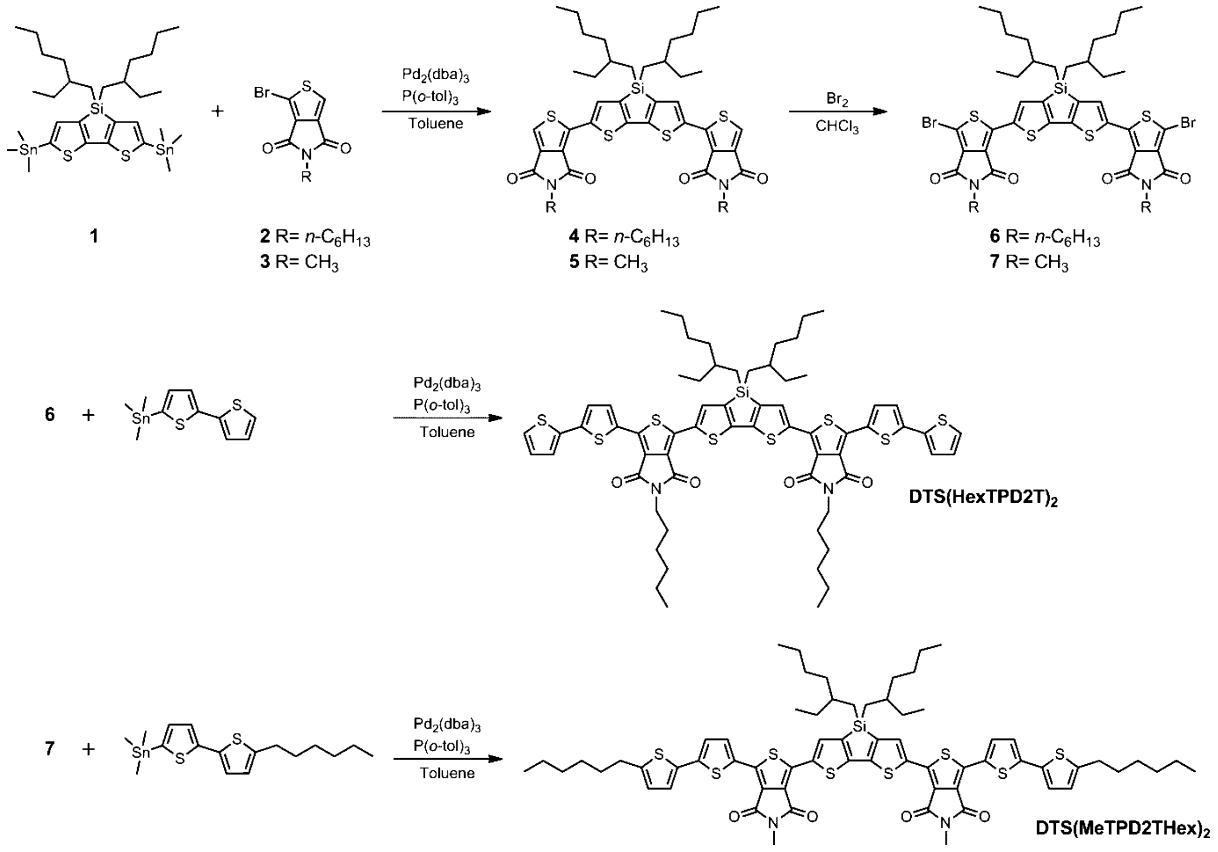

which are beneficial for high V_{OC} without causing bandgap widening. In short, TPD moiety as an A unit in a D−A-type conjugated backbone effectively lowers their HOMO energy levels without the sacrifice of bandgap widening, leading to high V_{OC} without any loss of short-circuit current (J_{SC}). This inspired us to design new TPD-based SMs to achieve high V_{OC} without significant sacrifice of J_{SC}.

On the other hand, DTS as a D unit has emerged as an important building block of semiconducting conjugated molecules for optoelectronic applications including field effect transistors (FETs) and OSCs. It has been demonstrated that DTS-containing polymers enhance the intermolecular ordering in the film state, compared to the polymer containing cyclopenta(2,1-*b*:3,4-*b*′)dithiophene, because of the long Si−C bond in the DTS unit, which allows efficient $\pi-\pi$ interaction.[22,23] Furthermore, the planar conjugated structure of the DTS unit affords effective intramolecular charge transfer through hybridization with an electron-accepting unit and thus the DTS-based molecules exhibit broad light-absorption and low-optical bandgap.[24−28] This advantage of the DTS unit leads to not only high hole mobility in FET (0.08 $cm^2\ V^{-1}\ s^{-1}$)[29] but also high PCE (7.3%) in OSCs.[21] Therefore, the DTS is a promising electron-donating unit of low-bandgap SMs for high-performance BHJ OSCs.

In this work, we designed and synthesized two SMs with a $D_1-A-D_2-A-D_1$ structure, where D_2 is DTS as a center and donating unit, A is TPD as an accepting unit, and D_1 is end-capping bithiophene (2T) as π-conjugation extender (Scheme 1). The chemical structures of two SMs differ only by the position of alkyl (hexyl) group substitution. The introduction of TPD in SMs is expected to lower HOMO energy level for achieving high V_{OC}. The SM with hexyl group substituted at the A unit showed a PCE of 6.0% with a high V_{OC} of 0.94 V in OSCs when blended with $PC_{71}BM$.

2. RESULTS AND DISCUSSION

Two SMs, 3,3′-(4,4-bis(2-ethylhexyl)-4H-silolo[3,2-*b*:4,5-*b*′]-dithiophene-2,6-diyl)bis(1-([2,2′-bithiophen]-5-yl)-5-hexyl-4H-thieno[3,4-*c*]pyrrole-4,6(5H)-dione) (**DTS(HexTPD2T)$_2$**) and 3,3′-(4,4-bis(2-ethylhexyl)-4H-silolo[3,2-*b*:4,5-*b*′]-dithiophene-2,6-diyl)bis(1-(5′-hexyl-[2,2′-bithiophen]-5-yl)-5-methyl-4H-thieno[3,4-*c*]pyrrole-4,6(5H)-dione) (**DTS(MeTPD2THex)$_2$**), were synthesized by the Stille cross-coupling reaction (Scheme 1). TPD-based SMs have rarely been reported, compared to corresponding polymer counterparts, probably because of limited synthetic procedures.[30−33] However, Leclerc and his co-workers[34−37] reported a useful method to synthesize *mono*-brominated TPD unit with various alkyl chains, leading to facile synthetic route of TPD-based SMs for OSC application. As shown in Scheme 1, compounds **2** and **3** were synthesized by following the Leclerc's procedure and then reacted with compound **1** to afford compounds **4** and **5** in 87% and 81% yield, respectively. Compounds **6** and **7** were prepared from the bromination of compounds **4** and **5** in chloroform (CF) and finally reacted with corresponding stannylated 2T to obtain the two SMs. The SMs with 2-ethylhexyl and *n*-hexyl group show good solubility in common solvents such as toluene, chlorobenzene (CB), and CF.

When the density functional theory (DFT) calculation at B3LYP/6-31G(d,p) basis set was performed to examine the electronic properties of the frontier orbital and optimized geometrical properties of the SMs, it reveals that the

distributions of HOMO and LUMO energy levels of both SMs are similar, as shown in Figure S1 in the Supporting Information. Both HOMO and LUMO wave functions delocalize over the entire π-conjugated backbone, indicating that strong intramolecular interaction takes place. When the dihedral angles between DTS, TPD, and T units as defined by θ_1, θ_2, and θ_3 in Figure S1 in the Supporting Information are calculated (see Table S1 in the Supporting Information), it reveals that the angles are very small, which is beneficial for chain ordering/packing in the film state.

The ultraviolet−visible light (UV-vis) absorption spectra of two SMs in CF solution and film state are represented in Figure 1 and the optical properties are summarized in Table 1. The

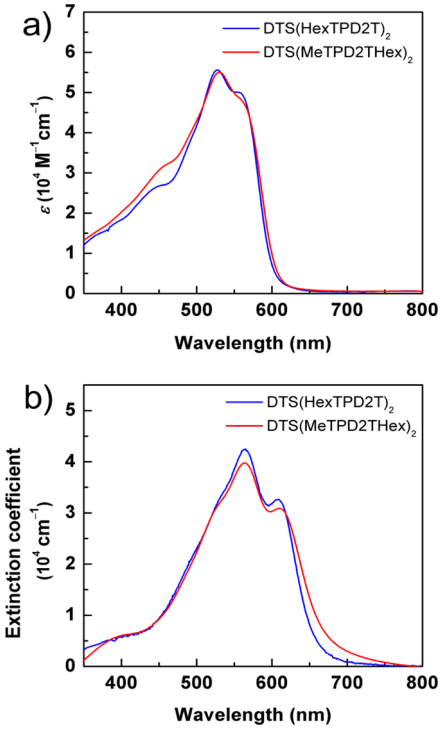

Figure 1. Ultraviolet−visible light (UV-vis) absorption spectra of SMs in (a) CF solution and (b) the film state.

molar extinction coefficients of two SMs at the maximum absorption wavelength (λ_{max}) of 530 nm are nearly equal (ca. 5.5×10^4 M^{-1} cm^{-1}) in solution, while the molar absorptivity of **DTS(HexTPD2T)$_2$** is slighly higher than that of **DTS(MeTPD2THex)$_2$** in solid film. The λ_{max} and the onset absorption wavelength (λ_{onset}) of two SMs in film state are red-shifted by ca. 35 and 60 nm, repectively, as compared to those in solution state. The optical band gaps (E_g^{opt}) of **DTS(HexTPD2T)$_2$** and **DTS(MeTPD2THex)$_2$**, as estimated from the corresponding λ_{onset}, are 1.86 and 1.85 eV, respectively. Particularly, two SMs show a strong vibronic shoulder in both solution and the solid film state, indicating that the two SMs are aggregated in both states.

The electrochemical properties of **DTS(HexTPD2T)$_2$** and **DTS(MeTPD2THex)$_2$** were measured by cyclic voltammetry (CV), as shown in Figure 2, and the results are summarized in

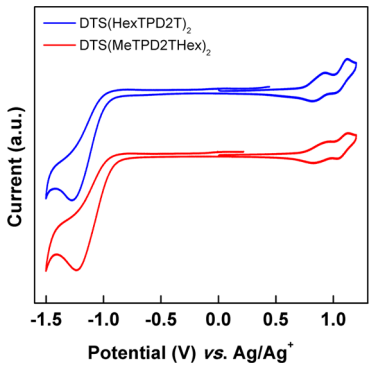

Figure 2. Cyclic voltammograms of SMs.

Table 1. The HOMO energy levels of two SMs are the same (−5.50 eV), while the LUMO energy level of **DTS(HexTPD2T)$_2$** is slightly higher than that of **DTS(MeTPD2THex)$_2$**. Particularly, the TPD unit lowers both the HOMO and LUMO energy level in D−A-type conjugated SMs, leading to enhancement of V_{OC}. It is also noted here that the low-lying LUMO energy levels of the SMs are still sufficiently higher than the LUMO energy level of $PC_{71}BM$ for efficient exciton dissociation.[38,39]

Photovoltaic performances of TPD-based SMs were measured with the conventional device structure, as shown in Figure 3, and the data are summarized in Table 2. The [6,6]-

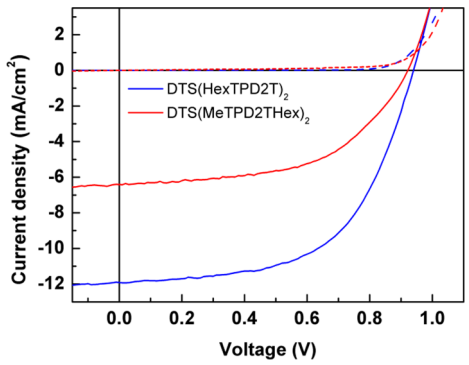

Figure 3. Current density−voltage (J−V) curves of **DTS(HexTPD2T)$_2$**:$PC_{71}BM$ (1.5:1) and **DTS(MeTPD2THex)$_2$**:$PC_{71}BM$ (1.5:1) BHJ solar cells processed with 0.5 vol % DIO under AM 1.5G, 100 mW cm^{-2}. The dashed lines are the corresponding dark currents.

phenyl-C_{71}-butyric acid methyl ester ($PC_{71}BM$) was used as an acceptor, because its absorptivity is higher than that of $PC_{61}BM$.

Table 1. Optical and Electrochemical Properties of Small Molecules (SMs)

SMs	UV-Vis Absorption		E_g^{opt} (eV)[a]	HOMO (eV)	LUMO (eV)	E_g^{el} (eV)[b]
	λ_{max} (solution) (nm)	λ_{max} (film) (nm)				
DTS(HexTPD2T)$_2$	528	564	1.86	−5.50	−3.78	1.72
DTS(MeTPD2THex)$_2$	530	565	1.85	−5.50	−3.83	1.67

[a]Determined from the onset of the UV-vis absorption spectra. [b]Determined from cyclic voltammetry.

Table 2. Photovoltaic Properties of OSCs Processed with 0.5 vol% DIO under AM 1.5G Illumination

SM	SM:$PC_{71}BM$ (w/w)	J_{SC} (mA cm^{-2})	V_{OC} (V)	fill factor, FF	$PCE_{max}(_{avg})^a$ (%)
DTS(HexTPD2T)$_2$^{b}	1.5:1	11.8	0.94	0.54	6.0 (5.8)
DTS(MeTPD2THex)$_2$^{c}	1.5:1	6.4	0.93	0.52	3.1 (2.8)

^{a}Average values of eight devices. ^{b}Chloroform (CF) solution. ^{c}Chlorobenzene (CB) solution.

The devices were optimized by varying processing conditions, such as the blend ratio and addition of solvent additives (see Figures S2–S4 and Table S2 in the Supporting Information). The PCEs of **DTS(HexTPD2T)$_2$** are always higher than that of **DTS(MeTPD2THex)$_2$**, regardless of the solvent, when the same solvent and additive are used. After the device optimization, the **DTS(HexTPD2T)$_2$**-based cell shows a promising PCE of 6.0% with V_{OC} = 0.94 V, J_{SC} = 11.8 mA cm^{-2}, and a fill factor (FF) of 0.54, which is one of the highest values of OSCs fabricated from TPD-based SMs, while **DTS(MeTPD2THex)$_2$** exhibits a moderate PCE of 3.1% with V_{OC} = 0.93 V, J_{SC} = 6.4 mA cm^{-2}, and FF = 0.52. It should be noted that all devices from two SMs exhibit high V_{OC} values of 0.93–0.94 V, which are originated from low-lying HOMO energy levels of the two SMs. The higher PCE of **DTS(HexTPD2T)$_2$** arises primarily from higher J_{SC}, as confirmed by external quantum efficiency (EQE) spectra (see Figure 4),

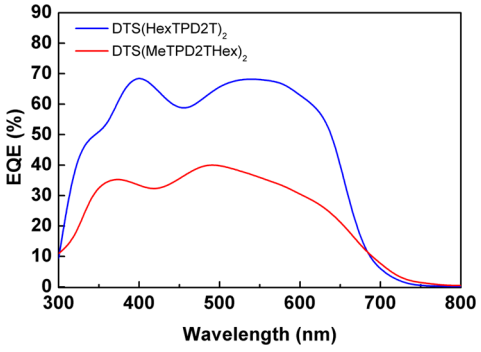

Figure 4. EQE spectra of **DTS(HexTPD2T)$_2$**:$PC_{71}BM$ (1.5:1 w/w) and **DTS(MeTPD2THex)$_2$**:$PC_{71}BM$ (1.5:1 w/w) BHJ solar cells.

where the **DTS(HexTPD2T)$_2$**-based device exhibits a stronger photoresponse in the range of 300–700 nm, which contributes to higher J_{SC} values in OSCs. The J_{SC} values calculated from integration of EQE curves of **DTS(HexTPD2T)$_2$** and **DTS(MeTPD2THex)$_2$** are 11.3 and 6.3 mA cm^{-2}, respectively, which are consistent with the values determined from the current density–voltage (J–V) curve.

While the optical and electrochemical properties of two SMs are nearly the same, regardless of the positon of alkyl chain substitution, photovoltaic properties of two SMs are largely different. To identify the reason for this large difference of photovoltaic properties, we compare the crystalline nature and molecular orientation of two SMs in film state. The grazing-incidence X-ray diffraction (GIXD) patterns of both **DTS(HexTPD2T)$_2$** and **DTS(MeTPD2THex)$_2$** show characteristic diffraction peaks—(100), (200), (300), and (400) in the q_z-direction and (010) in the q_{xy}-direction, indicating that the small molecules exhibit crystalline nature (see Figures 5a and 5b). However, it should be noted that **DTS(HexTPD2T)$_2$** molecules in the blend clearly exhibit a (010) peak at q = 1.78 $Å^{-1}$ along the q_z-direction while the **DTS(MeTPD2THex)$_2$** blend does not show a discernible peak at q = 1.78 $Å^{-1}$, as shown in Figures 5c and 5d, indicating that **DTS(HexTPD2T)$_2$** molecules take partially face-on orientation while **DTS(MeTPD2THex)$_2$** molecules do not clearly show face-on orientation. The out-of plane and in-plane scans also reveal that **DTS(HexTPD2T)$_2$** in the blend shows a (010) peak at q = 1.78 $Å^{-1}$ along the q_z- and q_{xy}-directions, as shown in Figures 5e and 5f, indicative of the existence of face-on orientation, which is advantageous for charge carrier transport in OSCs.[40−43] It is interesting to observe that **DTS(HexTPD2T)$_2$** has an interchain distance of 17.9 Å in the blend film, while **DTS(MeTPD2THex)$_2$** shows an interchain distance of 23.3 Å, indicating that the number of **DTS(HexTPD2T)$_2$** molecules per unit volume is larger than that of **DTS(MeTPD2THex)$_2$**, assuming that the two molecules have the same unit lengths along the (010) and (001) directions. In other words, the number of light-harvesting molecules of **DTS(HexTPD2T)$_2$** per unit volume is larger than that of **DTS(MeTPD2THex)$_2$**. It is noteworthy to mention here that the interchain distance of **DTS(HexTPD2T)$_2$** does not change, whereas that of **DTS(MeTPD2THex)$_2$** increases from 17.9 Å to 23.3 Å when they are blended with $PC_{71}BM$. Although we do not provide an exact reason for that, it is speculative that PCBM is more miscible with **DTS(MeTPD2THex)$_2$** than with **DTS(HexTPD2T)$_2$**, so that some of the PCBM molecules are intercalated between **DTS(MeTPD2THex)$_2$** molecules, which may increase the interchain distance. Considering that the PCE difference between the two SMs arises mainly from the J_{SC} difference, it is concluded that the more-preferential face-on

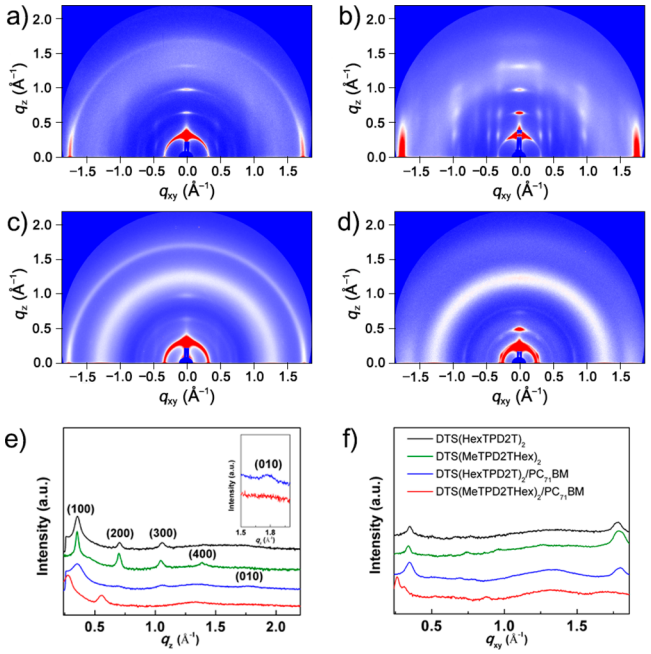

Figure 5. Two-dimensional grazing-incidence X-ray diffraction (2D-GIXD) images of (a) pristine **DTS(HexTPD2T)$_2$**, (b) pristine **DTS(MeTPD2THex)$_2$**, (c) **DTS(HexTPD2T)$_2$**:$PC_{71}BM$ (1.5:1 w/w) and (d) **DTS(MeTPD2THex)$_2$**:$PC_{71}BM$ (1.5:1 w/w) blends. Panels (e) and (f) respectively show out-of-plane and in-plane scans of pristine and blends.

orientation and larger number of light-harvesting molecules of **DTS(HexTPD2T)$_2$** crystal per unit volume, compared to those of **DTS(MeTPD2THex)$_2$**, contribute to the larger J_{SC} values.

When the hole mobilities of two SMs are measured by the space charge limited current (SCLC) method under the identical condition for optimized photovoltaic cell (Figure 6)

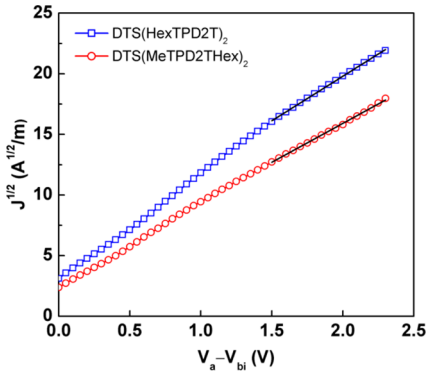

Figure 6. Dark J–V characteristics of **DTS(HexTPD2T)$_2$**:$PC_{71}BM$ (1.5:1 w/w), and **DTS(MeTPD2THex)$_2$**:$PC_{71}BM$ (1.5:1 w/w) blends with hole-only device. The solid lines represent the best linear fit of the data points.

and are compared, the hole mobility of **DTS(HexTPD2T)$_2$** (9.26×10^{-4} cm^2 V^{-1} s^{-1}) is higher than that of **DTS(MeTPD2THex)$_2$** (7.04×10^{-4} cm^2 V^{-1} s^{-1}). More preferential face-on orientation of **DTS(HexTPD2T)$_2$** in the blend as compared to **DTS(MeTPD2THex)$_2$** in the blend facilitates effective charge carrier transport, leading to a higher hole mobility in SCLC and, thus, higher J_{SC} values in OSCs.

To further investigate the J_{SC} difference between two small molecules, we examined the photoluminescence (PL) quenching of blend film (see Figure S5 in the Supporting Information). The PL of **DTS(HexTPD2T)$_2$** in the blend is almost completely quenched while that of **DTS(MeTPD2THex)$_2$** is quenched by 67%, indicating that the charge dissociation of excitons in **DTS(HexTPD2T)$_2$** occurs more efficiently than that of **DTS(MeTPD2THex)$_2$**, which also contributes to higher J_{SC} values of **DTS(HexTPD2T)$_2$**.

The J_{SC} values of OSCs are also dependent on the morphology of blend film. When the transmission electron microscopy (TEM) images of two SMs blended with $PC_{71}BM$ were compared, as shown in Figure 7, the **DTS(HexTPD2T)$_2$** blend reveals distinctly nanophase separated network while the **DTS(MeTPD2THex)$_2$** blend does show blurred phase

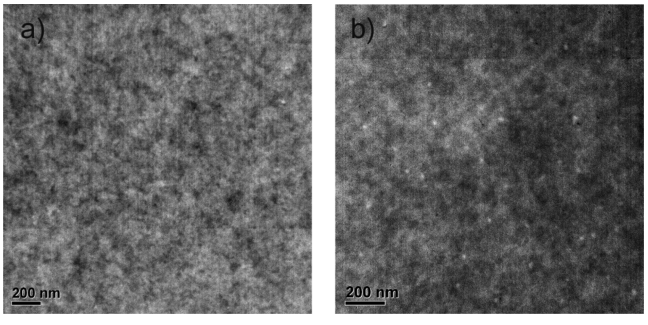

Figure 7. Transmission electron microscopy (TEM) images of (a) DTS(HexTPD2T)$_2$:$PC_{71}BM$ (1.5:1 w/w) and (b) DTS(MeTPD2THex)$_2$:$PC_{71}BM$ (1.5:1 w/w) blend films.

separation, indicating that the morphology of **DTS(HexTPD2T)$_2$** blend is more beneficial for charge transport than that of **DTS(MeTPD2THex)$_2$**. The above results of GIXD, the SCLC hole mobility, and TEM lead us to conclude that **DTS(HexTPD2T)$_2$** exhibits better photovoltaic performance than **DTS(MeTPD2THex)$_2$**.

3. CONCLUSION

Two SMs based on TPD unit with the same alkyl length but different substitution position are synthesized, and the effect of alkyl substitution position on their optical, electrochemical, and photovoltaic properties are examined. Since TPD, as an electron-accepting unit, lowers both HOMO and LUMO energy levels of D–A type conjugated polymers, we have introduced TPD unit into conjugated SMs for achieving high V_{OC} of OSCs without any significant loss of J_{SC}. As expected, two SMs exhibited low-lying HOMO (−5.50 eV) and LUMO (−3.83 eV) energy level, and thereby high V_{OC} of 0.93–0.94 V in OSCs. Although the optical and eletrochemical properties of the two SMs are almost the same, regardless of alkyl substitution position, photovoltaic performances of two SM:$PC_{71}BM$-based OSC devices are largely different. The **DTS(HexTPD2T)$_2$**-based OSC device exhibited a promising PCE of 6.0% with V_{OC} = 0.94 V, J_{SC} = 11.8 mA cm^{-2}, and FF = 0.54, while the **DTS(MeTPD2THex)$_2$**-based one showed a moderate PCE of 3.1% with V_{OC} = 0.93 V, J_{SC} = 6.4 mA cm^{-2}, and FF = 0.52. The larger J_{SC} value of **DTS(HexTPD2T)$_2$** is mainly attributed to the face-on orientation of crystallites, high SCLC hole mobility and nanoscaled phase separation observed in the blend. The PCE of 6.0% of **DTS(HexTPD2T)$_2$** is among the highest value of OSCs fabricated from TPD-based SMs.

4. EXPERIMENTAL SECTION

4.1. Materials. 2,2′-Bistrimethylstannyl-4,4′-bis(2-ethylhexyl)-dithieno[3,2-*b*:2′,3′-*d*]silole (**1**),[24] and 1-bromo-5-(alkyl)thieno[3,4-*c*]pyrrole-4,6-diones (**2**, **3**),[34] were synthesized following the same procedure as that reported in the literature. $Pd_2(dba)_3$, tri(*o*-toly)phosphine, and bromine were purchased from Sigma–Aldrich and used without further purification. Common organic solvents were purchased from Daejung. Poly(3,4-ethylenedioxythiophene):poly(styrenesulfonate) (PEDOT:PSS) (Clevios P VP AI 4083) was purchased from H.C. Starck and passed through a 0.45-μm PVDF syringe filter before spin coating. $PC_{71}BM$ was obtained from Nano-C. All other reagents were purchased from Tokyo Chemical Industry and used as received.

4.2. Synthesis. *4.2.1. Synthesis of 1,1′-(4,4-bis(2-ethylhexyl)-4H-silolo[3,2-b:4,5-b′]dithiophene-2,6-diyl)bis-(5-hexyl-4H-thieno[3,4-c]pyrrole-4,6(5H)-dione) (**4**, **5**).* Compound **1** (650 mg, 0.87 mmol), compound **2** (or **3**) (0.17 mmol), tri(*o*-tolyl)phosphine ($P(o\text{-toly})_3$) (21 mg, 0.06 mmol), and tris(dibenzylideneacetone)dipalladium(0) ($Pd_2(dba)_3$) (31 mg, 0.03 mmol) in anhydrous toluene (10 mL) were placed in a flask and stirred at 110 °C for 24 h under a N_2 atmosphere. The reaction mixture was poured into 200 mL of water and extracted with chloroform (CF). Organic phase was collected and dried over $MgSO_4$. The crude product was purified by column chromatography to yield compound **4** (or **5**).

Compound **4** (626 mg, 81% yield): ^{1}H NMR (300 MHz, $CDCl_3$, δ): 8.01 (t, 2H), 7.59 (s, 2H), 3.65 (t, 4H), 1.65 (d, 4H), 1.44–1.01 (m, 34H), 0.90–0.84 (t, 6H), 0.77 (t, 12H); ^{13}C NMR (500 MHz, $CDCl_3$, δ): 161.9, 161.6, 151.4, 148.4, 139.7, 137.3, 135.3, 130.5, 129.9, 122.4, 47.0, 40.1, 32.3, 31.1, 28.4, 28.1, 24.3, 23.5, 23.2, 22.9, 14.7, 14.4, 10.1, 9.8; MALDI-TOF MS m/z: calcd for $C_{48}H_{64}N_2O_4S_4Si$, 889.4; found, 890.3.

Compound **5** (475 mg, 73% yield): ^{1}H NMR (300 MHz, $CDCl_3$, δ): 8.02 (t, 2H), 7.60 (s, 2H), 3.16 (s, 6H), 1.44–1.01 (m, 22H), 0.78 (t, 12H); ^{13}C NMR (500 MHz, $CDCl_3$, δ): 162.7, 162.3, 150.7, 146.4,

139.9, 137.4, 134.8, 132.8, 127.1, 121.8, 35.8, 35.6, 28.8, 24.3, 22.9, 17.5, 14.1, 10.7; MALDI-TOF MS m/z: calcd for $C_{38}H_{44}N_2O_4S_4Si$, 749.1; found, 749.9.

*4.2.2. Synthesis of 3,3′-(4,4-bis(2-ethylhexyl)-4H-silolo[3,2-b:4,5-b′]dithiophene-2,6-diyl)bis-(1-bromo-5-alkyl-4H-thieno[3,4-c]-pyrrole-4,6(5H)-dione) (**6**, **7**).* After compound **4** (or **5**) (0.53 mmol) was dissolved in CF (20 mL), bromine (1.17 mmol) was added dropwise into the solution. The reaction mixture stirred for 30 min and then poured into 200 mL of water and extracted with CF. Organic phase was collected and dried over $MgSO_4$. The crude product was purified by column chromatography to yield compound **6** (or **7**).

Compound **6** (427 mg, 77% yield): ^{1}H NMR (300 MHz, $CDCl_3$, δ): 7.92 (t, 2H), 3.64 (t, 4H), 1.65 (d, 4H), 1.44−1.01 (m, 34H), 0.90−0.84 (t, 6H), 0.77 (t, 12H); 163.4, 162.1, 151.7, 148.1, 139.6, 137.3, 135.4, 130.6, 130.0, 122.4, 47.1, 40.3, 32.3, 31.1, 28.5, 28.1, 24.3, 23.4, 23.1, 22.9, 14.6, 14.5, 10.1, 9.9; MALDI-TOF MS m/z: calcd for $C_{48}H_{62}Br_2N_2O_4S_4Si$, 1047.2; found, 1048.3.

Compound **7** (475 mg, 73% yield): ^{1}H NMR (300 MHz, $CDCl_3$, δ): 7.92 (t, 2H), 3.15 (s, 6H), 1.42−1.00 (m, 22H), 0.78 (t, 12H); 163.5, 162.9, 151.1, 146.8, 139.9, 137.8, 134.8, 131.4, 126.5, 123.1, 35.7, 35.1, 28.4, 24.7, 22.6, 17.1, 14.5, 10.3; MALDI-TOF MS m/z: calcd for $C_{38}H_{42}Br_2N_2O_4S_4Si$, 906.9; found, 907.9.

*4.2.3. Synthesis of **DTS(HexTPD2T)$_2$**.* Compound **6** (400 mg, 0.38 mmol), [2,2′-bithiophen]-5-yltrimethylstannane (314 mg, 0.95 mmol), and P(*o*-toly)$_3$ (9.3 mg, 0.03 mmol) and $Pd_2(dba)_3$ (14.0 mg, 0.02 mmol) in anhydrous toluene (10 mL) were placed in a flask and stirred at 110 °C for 24 h under N_2 atmosphere. The reaction mixture was poured into 200 mL of water and extracted with CF. Organic phase was collected and dried over $MgSO_4$. The crude product was purified by column chromatography and recrystallization with *n*-hexane to obtain the **DTS(HexTPD2T)$_2$** (374 mg, 81% yield). ^{1}H NMR (300 MHz, $CDCl_3$, δ): 8.09 (t, 2H), 7.87 (d, 2H), 7.27 (d, 2H), 7.24 (d, 2H), 7.13 (d, 2H), 7.03 (q, 2H), 3.58 (t, 4H), 1.64 (m, 4H), 1.51 (m, 2H), 1.44−1.20 (m, 32H), 0.86 (m, 18H); ^{13}C NMR (500 MHz, $CDCl_3$, δ): 162.4, 151.2, 146.7, 141.2, 140.7, 136.5, 136.1, 135.5, 134.8, 133.1, 131.1, 130.8, 128.5, 128.1, 125.7, 124.8, 124.7, 124.0, 38.6, 35.9, 35.7, 31.4, 29.7, 29.0, 28.9, 28.5, 26.7, 23.0, 22.5, 17.7, 14.2, 14.0, 10.8; MALDI-TOF MS m/z: calcd for $C_{64}H_{72}N_2O_4S_8Si$, 1217.9; found, 1218.3. Anal. Calcd for $C_{64}H_{72}N_2O_4S_8Si$ (%): C, 63.12; H, 5.96; N, 2.30; O, 5.25; S, 21.06; Si, 2.31. Found (%): C, 63.08; H, 6.00.; N, 2.19; O, 5.29; S, 21.01; Si 2.34.

*4.2.4. Synthesis of **DTS(MeTPD2THex)$_2$**.* The same procedure as for **DTS(HexTPD2T)$_2$** was performed. The compound **7** (200 mg, 0.220 mmol) was reacted with (5′-hexyl-[2,2′-bithiophen]-5-yl)-trimethylstannane (200 mg, 0.485 mmol) in the presence of $Pd_2(dba)_3$ (8.0 mg, 0.008 mmol) and tri(*o*-tolyl)phosphine (5.3 mg, 0.016 mmol) in toluene (10 mL), to afford the product **DTS(MeTPD2THex)$_2$** (183 mg, 67% yield). ^{1}H NMR (300 MHz, $CDCl_3$, δ): 8.07 (d, 2H), 7.91 (d, 2H), 7.08 (d, 4H), 6.71 (d, 2H), 3.14 (s, 6H), 2.81 (t, 4H), 1.70 (m, 4H), 1.44−1.20 (m, 34H), 0.88 (t, 6H), 0.83 (t, 12H); ^{13}C NMR (500 MHz, $CDCl_3$, δ): 162.3, 151.4, 146.8, 141.2, 140.5, 136.8, 136.3, 135.7, 134.9, 133.2, 131.1, 130.7, 128.7, 128.3, 125.7, 124.7, 124.6, 124.1, 37.4, 33.4, 32.7, 32.0, 31.2, 29.7, 29.0, 28.9, 28.5, 26.7, 22.7, 20.4, 17.8, 14.3, 14.2, 10.7; MALDI-TOF MS m/z: calcd for $C_{64}H_{72}N_2O_4S_8Si$, 1244.3; found, 1244.7. Anal. Calcd for $C_{66}H_{76}N_2O_4S_8Si$ (%): C, 63.62 H, 6.15; N, 2.25; O, 5.14; S, 20.59; Si, 2.25. Found (%): C, 63.56; H, 6.19.; N, 2.29; O, 5.17; S, 20.51; Si 2.21.

4.3. Characterization and measurement. The chemical structures of compounds were identified by ^{1}H NMR (Avance DPX-300, Bruker) and ^{13}C NMR (Avance DPX-500, Bruker). Molar masses of compounds were measured by a matrix-assisted laser desorption/ionization time-of-flight (MALDI-TOF) mass spectrometer (Voyager-DE STR Biospectrometry Workstation, Applied Biosystem, Inc.) with dithranol as a matrix. The optical absorption spectra were obtained by a UV-vis spectrophotometer (Model Lambda 25, Perkin−Elmer). Cyclic voltammetry measurements were carried out using a potentiostat/galvanostat (Model VMP 3, Biologic) in an electrolyte solution of 0.1 M tetrabutylammonium hexafluorophosphate (Bu_4NPF_6) in dichloromethane. Platinum wires (Bioanalytical Systems, Inc.) were used as both counter and working electrodes, and silver/silver ion (Ag in 0.1 M $AgNO_3$ solution, Bioanalytical Systems, Inc.) was used as a reference electrode. Grazing-incidence X-ray diffraction (GIXD) experiments were performed at the PLS-II 9A U-SAXS beamline of Pohang Accelerator Laboratory (Korea). The X-rays coming from the in-vacuum undulator are monochromated (wavelength λ = 1.116 Å) using a double crystal monochromator and focused both horizontally and vertically (300 μm (H) × 30 μm (V) in fwhm at the sample position) using K−B-type mirrors. The GIXD sample state is equipped with a seven-axis motorized stage for accurate alignment, and the incidence angle of X-ray beam was set to 0.11° in this study. GIXD patterns were recorded with a 2D CCD detector (Raynoix SX165, USA) and X-ray irradiation time was 5−100 s, depending on the saturation level of the detector. Diffraction angles were calibrated by a precalibrated sucrose (monoclinic, P_{21}, a = 10.8631 Å, b = 8.7044 Å, c = 7.7624 Å, β = 102.938°), and the sample-to-detector distance was ∼230 mm. The morphology of active layer films was observed by TEM (Model JEM-1010, JEOL) with an accelerating voltage of 80 kV. Thickness of the active layers was measured by atomic force microscopy (Nano Xpert2).

4.4. Fabrication and Characterization of Photovoltaic Cells. The organic solar cells were fabricated with the standard device configuration of glass/ITO/PEDOT:PSS/SM:$PC_{71}BM$/Ca/Al. Prior to device fabrication, the ITO-coated glass was cleaned with acetone and then isopropyl alcohol for 15 min. After complete drying at 120 °C for 30 min, the ITO-coated glass was treated with UV-ozone for 10 min. PEDOT:PSS was spin-coated on the ITO glass at 3000 rpm for 40 s and annealed at 150 °C for 30 min to yield a film 30−40 nm thick. The devices were transferred into a glovebox filled with N_2. For preparation of SM and $PC_{71}BM$, **DTS(HexTPD2T)$_2$** was dissolved in CF (or with 0.5 vol % DIO as a solvent additive), and **DTS(MeTPD2THex)$_2$** was dissolved in CB (or with 0.5 vol % DIO). The solutions were stirred at 40 °C for 1 h and then spin-coated on the top of PEDOT:PSS. The thickness of resulting film is ca. 70−90 nm. Finally, calcium (20 nm) and then aluminum (100 nm) were thermally evaporated on the top of the active layer under vacuum (<10^{-6} Torr). The J−V characteristics were measured with a Keithley Model 4200 source-meter under AM 1.5 G (100 mW cm^{-2}) simulated by a Newport-Oriel solar simulator. The light intensity was calibrated using a NREL certified photodiode and a light source meter prior to each measurement. The active area is 10 mm^2. The EQE was measured using a lock-in amplifier with a current preamplifier (Model K3100, McScience Co.) under short-circuit current state with illumination of monochromatic light. The hole-only devices were fabricated with a device configuration of glass/ITO/PEDOT:PSS/SM:$PC_{71}BM$/Au. The hole mobilities of blend films were measured with the optimized photovoltaic devices prepared under identical conditions and calculated from the space-charge limited J−V curve, using the Mott−Gurney law.

■ ASSOCIATED CONTENT

Ⓢ Supporting Information

DFT calculation and additional photovoltaic data. This material is available free of charge via the Internet at http://pubs.acs.org.

■ AUTHOR INFORMATION

Corresponding Author

*Tel.: +82 2 880 7192. Fax: +82 2 876 6086. E-mail: whjpoly@snu.ac.kr.

Notes

The authors declare no competing financial interest.

■ ACKNOWLEDGMENTS

The authors thank the Ministry of Education, Science and Technology (MEST), Korea for financial support through Global Research Laboratory (GRL). Experiments at the PLS-II 9A U-SAXS beamline were supported in part by MIST and

POSTECH. The authors also thank Dr. Hyungju Ahn for GIXD measurement.

REFERENCES

(1) Kyaw, A. K. K.; Wang, D. H.; Gupta, V.; Leong, W. L.; Ke, L.; Bazan, G. C.; Heeger, A. J. Intensity Dependence of Current−Voltage Characteristics and Recombination in High-Efficiency Solution-Processed Small-Molecule Solar Cells. *ACS Nano* **2013**, *7*, 4569−4577.

(2) Zhou, J.; Zuo, Y.; Wan, X.; Long, G.; Zhang, Q.; Ni, W.; Liu, Y.; Li, Z.; He, G.; Li, C.; Kan, B.; Li, M.; Chen, Y. Solution-Processed and High-Performance Organic Solar Cells Using Small Molecules with a Benzodithiophene Unit. *J. Am. Chem. Soc.* **2013**, *135*, 8484−8487.

(3) Gupta, V.; Kyaw, A. K. K.; Wang, D. H.; Chand, S.; Bazan, G. C.; Heeger, A. J. Barium: An Efficient Cathode Layer for Bulk-Heterojunction Solar Cells. *Sci. Rep.* **2013**, *3*, 1965.

(4) Qin, H.; Li, L.; Guo, F.; Su, S.; Peng, J.; Cao, Y.; Peng, X. Solution-Processed Bulk Heterojunction Solar Cells Based on a Porphyrin Small Molecule with 7% Power Conversion Efficiency. *Energy Environ. Sci.* **2014**, *7*, 1397−1401.

(5) Liu, D.; Xiao, M.; Yan, Y.; Han, L.; Roy, V. A. L.; Sun, M.; Zhu, W.; Lee, C. S.; Yang, R. Solution-Processed, Indacenodithiophene-Based, Small-Molecule Organic Field-Effect Transistors and Solar Cells. *J. Mater. Chem. C* **2014**, *2*, 7523−7530.

(6) Bai, H.; Wang, T.; Cheng, P.; Li, Y.; Zhu, D.; Zhan, X. Acceptor-Donor-Acceptor Small Molecules Based on Indacenodithiophene for Efficient Organic Solar Cells. *ACS Appl. Mater. Interfaces* **2014**, *6*, 8426−8433.

(7) Harschneck, T.; Zhou, N.; Manley, E. F.; Lou, S. J.; Yu, X.; Butler, M. R.; Timalsina, A.; Turrisi, R.; Ratner, M. A.; Chen, L. X.; Chang, R. P. H.; Facchetti, A.; Marks, T. J. Substantial Photovoltaic Response and Morphology Tuning in Benzo[1,2-*b*:6,5-*b*′]dithiophene (bBDT) Molecular Donors. *Chem. Commun.* **2014**, *50*, 4099−4101.

(8) Yang, D.; Yang, Q.; Yang, L.; Luo, Q.; Chen, Y.; Zhu, Y.; Huang, Y.; Lu, Z.; Zhao, S. A Low Bandgap Asymmetrical Squaraine for High-Performance Solution-Processed Small Molecule Organic Solar Cells. *Chem. Commun.* **2014**, *50*, 9346−9348.

(9) Cui, C.; Min, J.; Ho, C.-L.; Ameri, T.; Yang, P.; Zhao, J.; Brabec, C. J.; Wong, W.-Y. A New Two-Dimensional Oligothiophene End-Capped with Alkyl Cyanoacetate Groups for Highly Efficient Solution-Processed Organic Solar Cells. *Chem. Commun.* **2013**, *49*, 4409−4411.

(10) Lan, S.-C.; Raghunath, P.; Lu, Y.-H.; Wang, T.-C.; Lin, S.-W.; Liu, C.-M.; Jiang, J.-M.; Lin, M.-C.; Wei, K.-W. Symmetry and Coplanarity of Organic Molecules Affect Their Packing and Photovoltaic Properties in Solution-Processed Solar Cells. *ACS Appl. Mater. Interfaces* **2014**, *6*, 9298−9306.

(11) Yu, Q.-C.; Fu, W.-F.; Wan, J.-H.; Wu, X.-F.; Shi, M.-M.; Chen, H.-Z. Evaluation of Heterocycle-Modified Pentathiophene-Based Molecular Donor Materials for Solar Cells. *ACS Appl. Mater. Interfaces* **2014**, *6*, 5798−5809.

(12) Lin, Y.; Ma, L.; Li, Y.; Liu, Y.; Zhu, D.; Zhan, X. A Solution-Processable Small Molecule Based on Benzodithiophene and Diketopyrrolopyrrole for High-Performance Organic Solar Cells. *Adv. Energy Mater.* **2013**, *3*, 1166−1170.

(13) Yuan, M.-C.; Chiu, M.-Y.; Liu, S.-P.; Chen, C.-M.; Wei, K.-H. A Thieno[3,4-*c*]pyrrole-4,6-dione-Based Donor−Acceptor Polymer Exhibiting High Crystallinity for Photovoltaic Applications. *Macromolecules* **2010**, *43*, 6936−6938.

(14) Su, M.-S.; Kuo, C.-Y.; Yuan, M.-Y.; Jeng, U.-S.; Su, C.-J.; Wei, K.-H. Improving Device Efficiency of Polymer/Fullerene Bulk Heterojunction Solar Cells Through Enhanced Crystallinity and Reduced Grain Boundaries Induced by Solvent Additives. *Adv. Mater.* **2011**, *23*, 3315−3319.

(15) Zhang, Y.; Zou, J.; Yip, H.-L.; Sun, Y.; Davies, J. A.; Chen, K.-S.; Acton, O.; Jen, A. K.-Y. Conjugated Polymers Based on C, Si and N-Bridged Bithiophene and Thienopyrroledione Units: Synthesis, Field-Effect Transistors and Bulk Heterojunction Polymer Solar Cells. *J. Mater. Chem.* **2011**, *21*, 3895−3902.

(16) Small, C. E.; Chen, S.; Subbiah, J.; Amb, C. M.; Tsang, S.-W.; Lai, T.-H.; Reynolds, J. R.; So, F. High-Efficiency Inverted Dithienogermole-Thienopyrrolodione-Based Polymer Solar Cells. *Nat. Photonics* **2011**, *6*, 115−120.

(17) Hong, Y.-R.; Wong, H.-K.; Moh, L. C. H.; Tan, H.-S.; Chen, Z.-K. Polymer Solar Cells Based on Copolymers of Dithieno[3,2-*b*:2′,3′-*d*]silole and Thienopyrroledione. *Chem. Commun.* **2011**, *47*, 4920−4922.

(18) Jo, J.; Pron, A.; Berrouard, P.; Leong, W. L.; Yuen, J. D.; Moon, J. S.; Leclerc, M.; Heeger, A. J. A New Terthiophene-Thienopyrrolodione Copolymer-Based Bulk Heterojunction Solar Cell with High Open-Circuit Voltage. *Adv. Energy Mater.* **2012**, *2*, 1397−1403.

(19) Liang, Y.; Xu, Z.; Xia, J.; Tsai, S.-T.; Wu, Y.; Li, G.; Ray, C.; Yu, L. For the Bright Future−Bulk Heterojunction Polymer Solar Cells with Power Conversion Efficiency of 7.4%. *Adv. Mater.* **2010**, *22*, E135−E138.

(20) Zou, Y.; Najari, A.; Berrouard, P.; Beaupré, S.; Aïch, B. R.; Tao, Y.; Leclerc, M. A Thieno[3,4-*c*]pyrrole-4,6-dione-Based Copolymer for Efficient Solar Cells. *J. Am. Chem. Soc.* **2010**, *132*, 5330−5331.

(21) Chu, T.-Y.; Lu, J.; Beaupré, S.; Zhang, Y.; Roulito, J.-R.; Wakim, S.; Zhou, J.; Leclerc, M.; Li, Z.; Ding, J.; Tao, Y. Bulk Heterojunction Solar Cells Using Thieno[3,4-*c*]pyrrole-4,6-dione and Dithieno[3,2-*b*:2′,3′-*d*]silole Copolymer with a Power Conversion Efficiency of 7.3%. *J. Am. Chem. Soc.* **2011**, *133*, 4250−4253.

(22) Chen, H.-Y.; Hou, J.; Hayden, A. E.; Yang, H.; Houk, K. N.; Yang, Y. Silicon Atom Substitution Enhances Interchain Packing in a Thiophene-Based Polymer System. *Adv. Mater.* **2010**, *22*, 371−375.

(23) Scharber, M. C.; Koppe, M.; Gao, J.; Cordella, F.; Loi, M. A.; Denk, P.; Morana, M.; Egelhaaf, H.-J.; Forberich, K.; Dennler, G.; Gaudiana, R.; Waller, D.; Zhu, Z.; Shi, X.; Brabec, C. J. Influence of the Bridging Atom on the Performance of a Low-Bandgap Bulk Heterojunction Solar Cell. *Adv. Mater.* **2010**, *22*, 367−370.

(24) Hou, J.; Chen, H.-Y.; Zhang, S.; Li, G.; Yang, Y. Synthesis, Characterization, and Photovoltaic Properties of a Low Band Gap Polymer Based on Silole-Containing Polythiophenes and 2,1,3-Benzothiadiazole. *J. Am. Chem. Soc.* **2008**, *130*, 16144.

(25) Ohshita, J. Conjugated Oligomers and Polymers Containing DithienoSilole Units. *Macromol. Chem. Phys.* **2009**, *210*, 1360−1370.

(26) Cui, C.; Fan, X.; Zhang, M.; Zhang, J.; Min, J.; Li, Y. A D−A Copolymer of Dithienosilole and a New Acceptor Unit of Naphtha-[2,3-*c*]thiophene-4,9-dione for Efficient Polymer Solar Cells. *Chem. Commun.* **2011**, *47*, 11345−11347.

(27) Ye, D.; Li, X.; Yan, L.; Zhang, W.; Hu, Z.; Liang, Y.; Fang, J.; Wong, W.-Y.; Wang, X. Dithienosilole-bridged Small Molecules with Different Alkyl Group Substituents for Organic Solar Cells Exhibiting High Open-Circuit Voltage. *J. Mater. Chem. A* **2013**, *1*, 7622−7629.

(28) Min, J.; Zhang, Z.-G.; Zhang, M.; Li, Y. Synthesis and Photovoltaic Properties of a D−A Copolymer of Dithienosilole and Fluorinated-Benzotriazole. *Polym. Chem.* **2013**, *4*, 1467−1473.

(29) Lu, G.; Usta, H.; Risko, C.; Wang, L.; Facchetti, A.; Ratner, M. A.; Marks, T. J. Synthesis, Characterization, and Transistor Response of Semiconducting Silole Polymer with Substantial Hole Mobility and Air Stability. Experiment and Theory. *J. Am. Chem. Soc.* **2008**, *130*, 7670−7685.

(30) Wang, H.-Y.; Cao, J.; Gu, L.-L; Wan, J.-H.; Wei, W.; Liu, F. Structural Modification of Thieno[3,4-*c*]pyrrole-4,6-dione: Structure−Property Relationships and Application in Solution-Processed Small Molecule Organic Solar Cells. *J. Mater. Chem. A* **2013**, *1*, 5875−5885.

(31) Ha, J.-J.; Kim, Y. J.; Park, J.-G.; An, T. K.; Kwon, S.-K.; Park, C. E.; Kim, Y.-H. Thieno[3,4-*c*]pyrrole-4,6-dione-Based Small Molecules for Highly Efficient Solution-Processed Organic Solar Cells. *Chem.—Asian J.* **2014**, *9*, 1045−1053.

(32) Kim, Y. J.; Park, K. H.; Ha, J.-J.; Chung, D. S.; Kim, Y.-H.; Park, C. E. The Effect of Branched *versus* Linear Alkyl Side Chains on the Bulk Heterojunction Photovoltaic Performance of Small Molecules Containing Both Benzodithiophene and Thienopyrroledione. *Phys. Chem. Chem. Phys.* **2014**, *16*, 19874−19883 (DOI: 10.1039/c4cp00077c).

(33) Kim, Y. J.; Baek, J. Y.; Ha, J.-J.; Chung, D. S.; Kwon, S.-K.; Park, C. E.; Kim, Y.-H. A High-Performance Solution-Processed Small

Molecules: Alkylselenophene-Substituted Benzodithiophene Organic Solar Cell. *J. Mater. Chem. C* **2014**, *2*, 4937−4946.
(34) Berrouard, P.; Grenier, F.; Pouliot, J.-R.; Gagnon, E.; Tessier, C.; Leclerc, M. Synthesis and Characterization of 5-Octylthieno[3,4-*c*]pyrrole-4,6-dione Derivative as New Monomers for Conjugated Copolymers. *Org. Lett.* **2011**, *13*, 38−41.
(35) Berrouard, P.; Dufresne, S.; Pron, A.; Veilleux, J.; Leclerc, M. Low-Cost Synthesis and Physical Characterization of Thieno[3,4-*c*]pyrrole-4,6-dione-Based Polymers. *J. Org. Chem.* **2012**, *77*, 8167−8173.
(36) Ottone, C.; Berrouard, P.; Louarn, G.; Beaupré, S.; Gendron, D.; Zagorska, M.; Rannou, P.; Najari, A.; Sadki, S.; Leclerc, M.; Pron, A. Donor−Acceptor Alternating Copolymers Containing Thienopyrrole-dione Electron Accepting Units: Preparation, Redox Behavior, and Application to Photovoltaic Cells. *Polym. Chem.* **2012**, *3*, 2355−2365.
(37) Pron, A.; Berrouard, P.; Leclerc, M. Thieno[3,4-*c*]pyrrole-4,6-dione-Based Polymers for Optoelectric Application. *Macromol. Chem. Phys.* **2013**, *214*, 7−16.
(38) Scharber, M. C.; Mühlbacher, D.; Koppe, M.; Denk, P.; Waldauf, C.; Heeger, A. J.; Brabec, C. Design Rules for Donors in Bulk-Heterojunction Solar Cells—Towards 10% Energy-Conversion Efficiency. *Adv. Mater.* **2006**, *18*, 789−794.
(39) Veldman, D.; Meskers, S. C. J.; Janssen, R. A. J. The Energy of Charge-Transfer States in Electron Donor−Acceptor Blends: Insight into the Energy Losses in Organic Solar Cells. *Adv. Funct. Mater.* **2009**, *13*, 1939−1948.
(40) Beiley, Z. M.; Hoke, E. T.; Noriega, R.; Dacuña, J.; Burkhard, G. F.; Bartelt, J. A.; Salleo, A.; Toney, M. F.; McGehee, M. D. Morphology-Dependent Trap Formation in High Performance Polymer Bulk Heterojunction Solar Cells. *Adv. Energy Mater.* **2011**, *1*, 954−962.
(41) Bartelt, J. A.; Beiley, Z. M.; Hoke, E. T.; Mateker, W. R.; Douglas, J. D.; Collins, B. A.; Tumbleston, J. R.; Graham, K. R.; Amassian, A.; Ade, H.; Frèchet, J. M. J.; Toney, M. F.; McGehee, M. D. The Importance of Fullerene Percolation in the Mixed Regions of Polymer−Fullerene Bulk Heterojunction Solar Cells. *Adv. Energy Mater.* **2013**, *3*, 364−374.
(42) Scarongella, M.; Paraecattil, A. A.; Buchaca-Domingo, E.; Douglas, J. D.; Beaupré, S.; McCarthy-Ward, T.; Heeney, M.; Moser, J.-E.; Leclerc, M.; Fréchet, J. M. J.; Stingelin, N.; Banerji, N. The Influence of Microstructure on Charge Separation Dynamics in Organic Bulk Heterojunction Materials for Solar Cell Applications. *J. Mater. Chem. A* **2014**, *2*, 6218−6230.
(43) He, M.; Wang, M.; Lin, C.; Lin, Z. Optimization of Molecular Organization and Nanoscale Morphology for High Performance Low Bandgap Polymer Solar Cells. *Nanoscale* **2014**, *6*, 3984−3994.